Research Square

Preprints are preliminary reports that have not undergone peer review.
They should not be considered conclusive, used to inform clinical practice,
or referenced by the media as validated information.

Comparison of Phosphate Adsorption on Synthetic and Naturally-Occurring Ferrihydrite by Surface Complexation Model

Jing Liu

liujing-vip@163.com

Southwest University

Shu Chen

Southwest University of Science and Technology

Research Article

Keywords: Ferrihydrite, Phosphate, Adsorption, Soil, Model

Posted Date: November 20th, 2026

DOI: https://doi.org/10.21203/rs.3.rs-11316090/v1

License: This work is licensed under a Creative Commons Attribution 4.0 International License.
Read Full License

Additional Declarations: No competing interests reported.

Abstract

Purpose

This study compares phosphate adsorption onto synthetic and field-derived 6-line ferrihydrite to develop a surface complexation model distinct from those established for 2-line ferrihydrite and to investigate the effects of coexisting ions on phosphate adsorption.

Methods

6-line ferrihydrite was synthesized in the laboratory, and natural 6-line ferrihydrite samples were collected from Shimen County, Changde, Hunan Province, China. Surface charge titration and batch adsorption experiments were conducted to investigate phosphate adsorption (1.07 mM PO_4^{3-}, pH 3-10.5). The adsorption behavior of coexisting ions, including SO_4^{2-} (3.7–23.6 μmol/L), AsO_4^{3-} (0.09–0.26 μmol/L), Ca^{2+} (0.10–0.84 μmol/L), and the combined presence of Ca^{2+} and SO_4^{2-}, was also examined. Corresponding surface complexation models (SCM) were developed, and the pH adsorption edges were simulated using FITEQL to determine the surface complexation constants.

Results

The surface protonation (pK_{a1}) and deprotonation (pK_{a2}) constants of the synthesized 6-line ferrihydrite were determined to be 6.80 and − 9.93, respectively, with a point of zero charge (PZC) of 8.5. The coexisting oxyanions SO_4^{2-} and AsO_4^{3-} inhibited phosphate adsorption on ferrihydrite, with maximum reductions of approximately 24% and 71%, respectively. In contrast, Ca^{2+} decreased phosphate adsorption by up to 25% under acidic conditions, but enhanced phosphate adsorption under alkaline conditions by as much as 95%. The combined presence of Ca^{2+} and SO_4^{2-} produced a pronounced synergistic effect and significantly altered the phosphate adsorption envelope of 6-line ferrihydrite. The resulting adsorption-envelope pattern closely resembled that observed for the natural 6-line ferrihydrite collected from a Ca^{2+}- and SO_4^{2-}-rich mining environment. The maximum phosphate adsorption capacities of the synthesized and natural ferrihydrite samples were 3.52×10^{-4} mol/L and 3.28×10^{-4} mol/L, respectively.

Conclusion

Although the active site concentration of the field-derived sample (2.67×10^{-3} mol site/mol Fe) was much lower than that of the laboratory-synthesized sample (2.00×10^{-2} mol site/mol Fe), the presence of coexisting ions enhanced its phosphate adsorption and altered the adsorption edge. These findings provide parameters for modeling the adsorption of coexisting ions on 6-lines ferrihydrite.

1. Introduction

Ferrihydrite is natural metastable iron oxyhydroxide with empirical formulas ($Fe_5HO_8{\cdot}4H_2O$) that is ubiquitous in some natural water and soil (Davis et al.1978; Schwertmann, 1985). Low temperature hydrolysis of Fe^{3+} or rapid oxidization of Fe^{2+} are the main mechanisms for its formation (Schwertamann et al. 1999). It is precisely these factors that lead to the coexistence of ferrihydrite and the ore stable goethite. Ferrihydirte occurs mainly in two mineral phases, 2-line and 6-line ferrihydrite due to their difference in 2 or 6–8 reflections in X-ray diffraction crystallinity (Michel et al., 2010). As a consequence, their specific surface areas and solubility are distinct (340–390 m^2/g and $K_{sp}=10^{-4.23\pm0.70}$ for 2-line ferrihydrite; 203–390 m^2/g and $K_{sp}=10^{-5.06\pm0.37}$ for 6-line ferrihydrite). Similar to hydrous ferric oxides (HFO), substantially more adsorption data and surface complexation models have been developed for 2-line ferrihydirte than 6-line ferrihydrite. Recent filed studies in mining area have also documented the presence of 6-line ferrihydirte (Fan et al., 2018; Ren et al., 2022).

Phosphate (PO_4^{3-}) is penta-oxyanion ubiquitous in aquatic and terrestrial environments, sharing structural similarities with other environmentally relevant oxyanions such as arsenate (AsO_4^{3-}), silicate (SiO_4^{3-}), and vanadate (VO_4^{3-}) (Antelo et al., 2015). Its strong electrostatic interactions and pronounced tendency for inner-sphere complexation with Fe- and Al-(hydr)oxide surfaces result in efficient adsorption, rendering phosphate a key regulator of phosphorus mobility and biogeochemical transformation processes.

Adsorption behavior and mechanism of specific phosphate on iron oxide minerals has been extensively and continuously investigated over the past decades, ranging from constant capacity model (CCM) (Goldberge, 1985; Hayes et al., 1988; Nilsson et al., 1996; Nowack et al., 2006; Gauthier, 2011; Loannou et al, 2013; Liang et al., 2024), triple-layer model (TLM) (Hawke, et al., 1989; Gao and Mucci, 2001; Kanematsu et al. 2010 and 2011) and the charge distribution multi-site complexation (CD-MUSIC) model (Venema et al. 1997; Hiemstra and Zhao, 2016; Talebi et al., 2016; Mendez et al., 2019, 2020;). The adsorption of phosphate anions at aqueous solution and iron oxides interfaces involves formation of inner sphere coordination complexes on the surface of the minerals (Dzombak et al., 1990).

The phosphate adsorption envelope on iron minerals is governed by pH-dependent changes in surface protonation states and the extent of ligand-exchange complexation at reactive surface sites. Comparison of adsorption envelope under different conditions provide clearer insight into variations in adsorption behavior and underlying mechanisms. CCM has been used to describe phosphate adsorption using ligand exchange mechanism for Fe/Al oxides and soils (Goldberg, 1984a and 1984b; Verbeeck et al., 2017; Tiberg et al., 2020). The dominant adsorbed species are protonated mononuclear surface complexes. The spectroscopic evidence suggests that bidentate phosphate complexes may form under conditions of elevated phosphate loading. But this is good agreement between the models and thermodynamic and infrared spectroscopy data, presented by various authors at low phosphate

conditions (< 0.8mmol/L) (Sigg et al., 1981; Goldberg, et al, 1984, Nilsson, 1996; Tejedor-Tejedor, et al., 1990; Persson, et al., 1996;).

The primary objective of this study is to investigate the pH-dependent adsorption behavior of phosphate on laboratory-synthesized 6-line ferrihydrite and to evaluate the effects of coexisting species under binary systems. In parallel, 6-line ferrihydrite samples collected from the reaglar mine area, Shimen country, Changde city, Hunan province were examined for comparison, thereby establishing a linkage between controlled laboratory systems and field-relevant conditions to improve the understanding on the mechanisms governing phosphate adsorption.

2. Materials and methods

2.1 synthesis of 6-lines ferrihydrite

Ferrihdyrite is the iron oxides and was chosen as the model iron oxide to study the adsorption behavior of phosphate. Since the ferrihydrite in the mine area is 6-line ferrihydrite, this study also synthesized 6-line ferrihydrite using the method proposed by Cornell and Schermann et al. 2003. The specific synthesis procedure is as follows: 20 grams of iron(III) nitrate nonahydrate ($Fe(NO_3)_3{\cdot}9H_2O$) are added to a 2-liter beaker containing deionized water preheated to 75°C. The beaker is placed on an IKA magnetic heating plate and stirred vigorously with a glass rod several times. The entire setup is then transferred into an oven maintained at 75°C for 10–12 minutes. After removal, the solution is immediately quenched in an ice-water bath for rapid cooling. The dark red solution is subsequently transferred into a dialysis bag with a molecular weight cutoff of 3,500 Da. The dialysate is replaced with fresh water twice daily until the conductivity of the solution drops below 2 μS/m, typically requiring approximately 5 days to complete the process. The samples was freezed dried (Labonco, FreeZone, USA) and then ground with a mortar and pestle for later adsorption and characterization use.

2.2 Acid-base titration

The titrations of 6-lines ferrihydrite were conducted in double layer glass vessel, which was surrounded with 25°C circulating water from a circulating condenser (Pharmaci Biotech MultiTemp III). 0.0960 g 6-lines ferrihydrite and 40 mL background electrolyte were added to the vessel and equilibrated for 1 hour. The electrolyte was sparged with high purity argon gas for 2 hours assuring the system was free of CO_2. The pH electrode (Metter Toledo DGi111-SC) is calibrated using four-point pH buffer soutions(1.68, 4.01, 7.00 and 9.20) before use. The Metter Toledo potentiometric titrator (T50) is used for dynamic monitoring and data recording. The titrations were run form the starting pH of about 3.2 up to a pH of 9.2 with 0.1000M HNO_3 and 0.0200M NaOH. Total proton concentration (TOTH) was calculated as following equation (Herbelin and Westall, 1999):

$$\mathrm{TOTH} = \frac{C_a V_a - C_b V_b}{V_0 + V_a + V_b}$$ Eq. 1

Where C_a and C_b are the concentration of standard acid and base, V_a and V_b is the total volume of standard acid use in titration and the cumulative volume of base added at each titration point, V_0 is the initial volume of the ferrihydrite suspension system. The factor of dilution (D) in the titration is calculated as following equation Herbelin and Westall, 1999):

$$\mathrm{D} = \frac{V_0+V_a}{V_0+V_a+V_b} \quad \text{Eq. 2}$$

The acidity constants were generated by FITEQL fitting of three sets of titration data.

2.3 pH envelope adsorption of phosphate on 6-lines ferrihydrite

The pH envelope adsorption of phosphate on ferrihydrite was investigated at the constant concentration of PO_4^{3-}. The stock solutions of PO_4^{3-}, $NaNO_3$, SO_4^{2-}, AsO_4^{3-} and Ca^{2+} were prepared by dissolving guaranteed reagents NaH_2PO_4, $NaNO_3$, Na_2SO_4, $Na_2HAsO_4{\cdot}7H_2O$ and $Ca(NO_3)_2$ (Alfa Aesar company), respectively. Appropriate volume of various stock solutions were added into 1L volumetric flask to obtained the constant initial PO_4^{3-} concentration of 1.07 μmol/L, 0.01 M $NaNO_3$ background and others different initial concentrations of SO_4^{2-}, AsO_4^{3-} and Ca^{2+}. ~ 60 mL initial solution was adjusted to the desired initial pH range (3.5–10.5) using 0.1 M HCl and 0.1 M NaOH. Take 25 mL of the above solution into a 50 mL centrifuge tube and run parallel simultaneously. 60 mg ferrihydrite was added into each tube and agitated at 150 rpm and 25 °C. The solutions were filtered using 0.45 μm membrane filters after 24 hrs and analyzed for PO_4^{3-} using Inductively Coupled Plasma Optical Emission Spectrometry (ICP-OES, iCAP6500 ThermoFisher) (Clesceri et al., 1989). The adsorbed PO_4 was obtained from the difference between the initially added and final concentrations of PO_4 in the equilibrium solution.

2.4 Determination and optimization of Equilibrium constants

The adsorption envelopes of phosphate were fitted based on an iterative approach of a nonlinear least-squares fitting grogram FITEQL, which achieved by best fit proton binding constants and the equilibrium intrinsic constants for the complexation of 6-lines ferrihydrite with phosphate (Herbelin and Westall, 1996). FITEQL grogram was developed based on the computer program MICROQL (Westall, 1979). The constant capacity model was adopted in this study.

2.5 Collection and subsequence use of 6-ferrihydrite from realgar mine area

The natural ferrihydrite was collected from historical Shimen realgar mine area (29°38'11" – 29°38'43"N, 111°2'06" – 111°2'23"E), Changde City, Hunan province, China. The Long-term beneficiation and separation processes of realgar raw ore and abundant occurrence of carbonate strata ($CaCO_3$ and $CaMg(CO_3)_2$), together with the initial water treatment by adding ferric sulfate ($Fe_2(SO_4)_3$), have led to the

formation of two kinds main secondary minerals including ferrihydrite and gypsum ($CaSO_4 \cdot 2H_2O$). About ~ $2.7 \cdot 10^5$ tons ferrihydrite tailings in this area will need to be storage or disposed.

40 g of the collected sample were suspended in 1 L of deionized water (> 18 MΩ·cm resistivity) and transferred to a glass graduated cylinder, where the suspension was allowed to settle for 4 min. Subsequently, 26.0 cm of the supernatant was decanted from the top of the suspension in the graduated cylinder. Particles with a diameter of approximately 8 μm were collected and dried for subsequent use. The mineralogical phases of samples was determined to be both 6-lines ferrihydrite and gypsum by X-ray diffraction (X'Pert PRO, PANalytical) and MDI Jade 5.0 softwarere. The titration and adsorption experiments were carried out in the same as those for the synthesized ferrihydrite above.

3. Results and discussions

3.1 Mineralogical characterization

The XRD results showed that the mineral synthesized following the method of Schwertmann and Cornell (1991) exhibited relatively distinct characteristic peaks at approximately 35°, 41°, 46°, 51°, 53°, and 63°. Due to its low crystallinity, the mineral displayed weak and broad diffraction peaks, confirming that it was 6-line ferrihydrite (Fig. 1a). For the field-collected samples, XRD analysis after sedimentation-based extraction showed diffraction patterns consistent with 6-line ferrihydrite, with a minor amount of gypsum also detected (Fig. 1b). Fan et al. (2018) suggested that the amorphous nature and encapsulation characteristics of ferrihydrite make it difficult to obtain gypsum-free samples through high-speed centrifugation and sedimentation.

3.1 Acid-base titrations

The acid-base titration curves of the synthesized 6-lines ferrihydrite under different ionic strengths (0.1, 0.01 and 0.001 M $NaNO_3$) are shown in Fig. 2. The curves are presented as pH versus total added proton concentration (TOTH, mol/L). As pH increased, TOTH gradually decreased, indicating progressive deprotonation of surface hydroxyl groups. The three curves intersected at approximately pH 8.5, suggesting that the point of zero charge (PZC) of 6-lines ferrihydrite is 8.5. Xu et al. (2011) suggested that ferrihydrite contains only a small amount of structural hydroxyl groups (Xu et al., 2011). Therefore, the protonation and deprotonation behavior of ferrihydrite is largely governed by the hydration of surface Fe atoms, which in turn affects its point of zero charge (PZC). This values is higher than HFO 8.1 (Dzombak and Morel, 1990; Monika, 2008) and 2-lines ferrihydrite 8.1 (Dzombak and Morel, 1990; Mendez et al., 2020) and lower than goethite (9.5 for Mesuere et Fishe, 1992 9.1 for Monika, 2008). The ferrihydrite surface was dominated by positive charges, whereas negative surface sites became dominant above this pH. Similar amphoteric surface behavior has been widely reported for ferrihydrite and other iron oxyhydroxides (Dzombak and Morel, 1990; Cornell and Schwertmann, 2003).The higher PZC value observed in this study compared with Si-ferrihydrite reported by Anderson and Benjamin (1985, pH□zc = 6.2) and Schwertmann and Fechter (1982, pH□zc = 6.1) may be related to differences in

crystallinity, silicate incorporation, and surface hydroxyl density. In addition, higher ionic strength resulted in greater proton consumption at low pH, indicating compression of the electrical double layer and enhanced surface protonation, which is consistent with previous studies on ferrihydrite surface charging behavior (Hiemstra and van Riemsdijk, 1996; Liu et al., 2008; Hiemstra and Riemsdijk, 2009; Hiemstra, 2013; Hiemstr and Riemsdijk, 2016).

The obtained intrinsic protonation constant (pK_{a1}^{int}) and intrinsic deprotonation constant (pK_{a2}^{int}) were 6.80 and 9.93, respectively. These values were used in all subsequent CCD model. The corresponding constants reported for 2-line ferrihydrite are 7.29 and 8.93, whereas those for goethite are 7.90 and 10.70. The optimized surface-site density was 2.00×10^{-2} mol site/mol Fe. This value is higher than the 1.50×10^{-2} mol site/mol Fe reported for goethite by Mesuere and Fish (1992) using the diffuse-layer model, but is well agreement with the 2.00×10^{-2} mol site/mol Fe reported for 2-line ferrihydrite by Dzombak and Morel (1990) and the 2.00×10^{-2} mol site/mol Fe obtained for lepidocrocite by Davies (1987).

3.2 Adsorption and CCM

3.2.1 Effect of SO_4^{2-}

Table 1
Summary of equilibrium surface adsorption and precipitation reaction and intrinsic equilibrium constants used to model phosphate adsorption on 6-lines ferrihydrite

Equilibrium reaction	Adsorption site	Intrinsic constant (log)	Equilibrium reaction	Adsorption site	Intrinsic constant (log)
$\equiv FeOH + H^+ \rightleftharpoons \equiv FeOH_2^+$	Mineral Surface	*6.80* §	$\equiv FeOH + Ca^{2+} \rightleftharpoons \equiv FeO^-Ca^{2+} + H^+$	β	-5.00
$\equiv FeOH \rightleftharpoons \equiv FeO^- + H^+$	Mineral surface	*-9.93* §	$\equiv FeOH + H^+ + PO_4^{3-} \rightleftharpoons \equiv FePO_4^{2-} + H_2O$	Mineral surface	Fit
$H^+ + PO_4^{3-} \rightleftharpoons HPO_4^{2-}$	Solution	*12.35* ‡	$\equiv FeOH + 2H^+ + PO_4^{3-} \rightleftharpoons \equiv FeHPO_4^- + H_2O$	Mineral Surface	Fit
$2H^+ + PO_4^{3-} \rightleftharpoons H_2PO_4^-$	Solution	*19.55* ‡	$\equiv FeOH + 3H^+ + PO_4^{3-} \rightleftharpoons \equiv FeH_2PO_4^0 + H_2O$	Mineral Surface	Fit
$3H^+ + PO_4^{3-} \rightleftharpoons H_3PO_4^0$	Solution	*21.70* ‡	$\equiv FeOH + H^+ + AsO_4^{3-} \rightleftharpoons \equiv FeAsO_4^{2-} + H_2O$	Mineral Surface	-0.63 ¶
$H^+ + AsO_4^{3-} \rightleftharpoons HAsO_4^{2-}$	Solution	*11.50* ‡	$\equiv FeOH + 2H^+ + AsO_4^{3-} \rightleftharpoons \equiv FeHAsO_4^- + H_2O$	Mineral Surface	*5.80* ¶
$2H^+ + AsO_4^{3-} \rightleftharpoons H_2AsO_4^-$	Solution	*18.46* ‡	$\equiv FeOH + 3H^+ + AsO_4^{3-} \rightleftharpoons \equiv FeH_2AsO_4^0 + H_2O$	Mineral Surface	*10.10* ¶

§ Obtained from titration data;

‡ Dzombak and Morel (1990**);**

¶ Goldberg (1985a**);**

† From optimization;

Equilibrium reaction	Adsorption site	Intrinsic constant (log)	Equilibrium reaction	Adsorption site	Intrinsic constant (log)
≡FeOH + H^+ ⇌ ≡$FeOH_2^+$	**Mineral Surface**	***6.80* §**	**≡FeOH + Ca^{2+}⇌ ≡FeO^-Ca^{2+} + H^+**	**β**	**-5.00**
3H^+ + AsO_4^{3-}⇌ $H_3AsO_4^0$	**Solution**	*20.70* ‡	**FeOH + H + + Ca^{2+} + SO_4^{2-} ⇌ $FeOH_2^+CaSO_4$**	**β**	**11.70**
≡FeOH + H^++SO_4^{2-} ⇌ ≡$FeSO_4$- + H_2O	**Mineral Surface**	*7.78* ‡	**FeOH + PO_4^{3-}+ H^+ + Ca^{2+} ⇌ $FePO_4^{2-}Ca$ + H_2O**	**Mineral Surface**	**Fit**
≡FeOH +$SO4^{2-}$ ⇌ ≡FeOH$SO_4$2-	**Mineral Surface**	*0.79* ‡	**Other parameters used in Model** **Surface area (m^2/g): 115** **Suspension density (g/L): 2.4** **Capacitance values (F/m^2): 1.05** **Maximum adsorption density (mol/m^3): 3.48 †**		
§ Obtained from titration data;					
‡ Dzombak and Morel (1990**);**					
¶ Goldberg (1985a**);**					
† From optimization;					

The adsorption of phosphate onto ferrihydrite remained relatively stable from pH 3 to 6, showed a pronounced decline between pH 7 and 9, and leveled off again at pH values above 10 (Fig. 3). Model fitting yielded a reactive sites concentration of 3.488 × 10^{-4} mol/L. The optimized phosphate surface-complexation constants obtained from the adsorption-envelope modeling were log Kp_1=31.48, logKp_2=24.99, and logKp_3=19.65. For comparison, the corresponding values reported for hydrous ferric oxide (HFO) by Dzombak and Morel (1990) were 31.29, 25.39, and 17.72, respectively. For goethite, Nilsson et al. (1996) reported values of 32.25, 27.50, and 21.73, whereas Nowack and Stone (2006) reported 31.64, 25.68, and 18.86, and Gauthier (2011) reported 31.05, 25.44, and 19.12. Wang et al. (2013) reported that the phosphate adsorption capacity of two-line ferrihydrite with different degrees of crystallinity ranged from 980 to 1690 μmol/g at pH 4.5 in 0.01 M KCl, while their specific surface areas varied from 234 to 427 m^2/g (Wang et al., 2013). In the present study, the phosphate adsorption capacity of 6-line ferrihydrite was 352 μmol/g.

Sulfate exerted a measurable inhibitory effect on phosphate adsorption throughout the adsorption envelope. Relative to the sulfate-free group, the average phosphate adsorption decreased by approximately 21%, 30%, and 49% at sulfate concentrations of 3.7, 10.2, and 23.6 μmol/L respectively. The magnitude of inhibition increased monotonically with sulfate concentration, demonstrating a clear concentration-dependent competitive effect. Incorporation of the sulfate competitive adsorption-site mechanism (Table 1) significantly improved the CCD model fit to the experimental adsorption data. Consequently, this mechanism was retained in all subsequent model calculations.

The adsorption-envelope results indicated that the presence of sulfate inhibited phosphate adsorption on ferrihydrite. At pH 10.5, the adsorbed phosphate concentration decreased from 1.86×10^{-4} mol/L in the sulfate-free system to 5.06×10^{-5} mol/L in the system containing 3.7 μmol/L sulfate, representing a decrease of approximately 72.8% (Fig. 3). As the sulfate concentration further increased, this promoting effect became weaker, and the equilibrium phosphate concentrations were 1.28×10^{-4} mol/L and 1.10×10^{-4} mol/L in the presence of 10.2 μmol/L and 23.6 μmol/L sulfate, respectively. The maximum reductions in equilibrium phosphate concentration were observed under alkaline conditions (pH ≈ 10.5) (Fig. 3). Specifically, the equilibrium phosphate concentration decreased by 72.8%, 31.2%, and 40.9% in the presence of 3.7, 10.2, and 23.6 μmol/L sulfate, respectively. The enhancement effect followed the order: 3.7 μmol/L SO_4^{2-}> 23.6 μmol/L SO_4^{2-} > 10.2 μmol/L SO_4^{2-}.

Notably, the adsorption envelope obtained in the presence of 10.2 μmol/L sulfate was closer to that of the sulfate-free system than the adsorption envelope obtained in the presence of 23.6 μmol/L sulfate. This phenomenon may be attributed to the suppression of phosphate adsorption by low concentrations of sulfate through alteration of the surface electrostatic properties, whereas higher sulfate concentrations may also suppress adsorption by occupying a portion of the active sites. For the adsorption envelope obtained at 23.6 μmol/L SO_4^{2-}, the model achieved a better fit when the competitive adsorption of sulfate was taken into account (Fig. 3).

3.2.2 Effect of AsO_4^{3-}

The presence of arsenate caused a systematic decrease in phosphate adsorption over the entire adsorption envelope. Compared with the arsenate-free system, phosphate adsorption was reduced by an average of approximately 18%, 28%, and 48% in the presence of 0.09, 0.129, and 0.258 μmol/L AsO_4^{3-}, respectively. Arsenate exhibited a substantially stronger competitive effect on phosphate adsorption than sulfate at comparable concentrations (Fig. 4).

3.2.3 Effect of Ca^{2+}

Ca^{2+} exhibited a distinctly different effect from sulfate and arsenate. Rather than suppressing phosphate adsorption, Ca^{2+} enhanced phosphate retention on ferrihydrite, particularly under alkaline conditions. Relative to the Ca-free system, phosphate adsorption increased by approximately 15%, 10% and 65% on

average in the pH range above 8 in the presence of 0.10, 0.46 and 0.84 mmol/L Ca^{2+}, respectively (Fig. 5). The enhancement became increasingly pronounced with increasing calcium concentration, with the strongest effect observed at 0.84 mmol/L Ca^{2+}. Furthermore, the model incorporating the contribution of surface precipitation was able to well fit the experimental data. Weng et al. (2012) found that the presence of Ca^{2+} alters the shape of the phosphate adsorption envelope on ferrihydrite (Weng et al., 2012). The present study further demonstrates that, under acidic conditions, Ca^{2+} tends to occupy shared adsorption sites, thereby decreasing phosphate adsorption onto ferrihydrite, whereas under alkaline conditions, Ca^{2+} enhances phosphate adsorption.

3.2.3 Synergistic effect of Ca^{2+} and SO_4^{2-}

The combined presence of Ca^{2+} and SO_4^{2-} exerted a concentration-dependent influence on phosphate adsorption by ferrihydrite. In the system containing 0.10 mmol/L Ca^{2+} and 3.7 μmol/L SO_4^{2-}, phosphate adsorption was enhanced by approximately 15–25% under alkaline conditions relative to the ion-free system (Fig. 6). At intermediate concentrations (0.46 mmol/L Ca^{2+} and 10.2 μmol/L SO_4^{2-}), the enhancement became much less pronounced, indicating that sulfate competition partially counteracted the promoting effect of calcium. In contrast, the system containing 0.84 mmol/L Ca^{2+} and 23.6 μmol/L SO_4^{2-} exhibited the strongest enhancement, with phosphate adsorption increasing by approximately 70–90% at pH values above 8 (Fig. 6). The synergistic enhancement of phosphate adsorption on ferrihydrite observed in the presence of 0.84 mmol/L Ca^{2+} and 23.6 μmol/L SO_4^{2-} was greater than that induced by 0.84 mmol/L Ca^{2+} alone.

Compared with the single-ion systems, the adsorption behavior in the mixed Ca-SO_4 systems was primarily controlled by calcium under alkaline conditions. Although sulfate alone suppressed phosphate adsorption, its inhibitory effect was progressively overcome by increasing Ca^{2+} concentration. At the highest Ca^{2+} level, the enhancement exceeded that observed in the corresponding single-Ca system, suggesting that calcium-mediated ternary surface complexes and/or Ca-phosphate surface precipitates became increasingly important contributors to phosphate retention on ferrihydrite.

3.3 Adsorption of phosphate on natural ferrihydrite

The samples collected from the Shimen mining area consisted primarily of a mixture of 6-line ferrihydrite and gypsum (Fig. 7). Consequently, Ca^{2+} and SO_4^{2-} are commol/Lon coexisting ions in this environment. In addition, arsenic-bearing minerals, particularly realgar, are abundant in the study area, resulting in a measurable arsenic content in the samples (As_2O_3 = 4.83% (wt.), determined by XRF analysis). The phosphate adsorption envelope of the natural sample differed markedly from that of the laboratory-synthesized 6-line ferrihydrite (Fig. 8). Phosphate adsorption increased progressively from 1.02×10^{-5} mol/L to 3.28×10^{-4} mol/L, with the maximum adsorption capacity approaching that of the synthesized

6-line ferrihydrite (3.52×10^{-4} mol/L). However, the maximum adsorption for the Shimen sample occurred at pH 10.46, whereas the synthesized 6-line ferrihydrite exhibited its maximum adsorption at pH 3.05.

Considering the synergistic effects of Ca^{2+} and SO_4^{2-} on phosphate adsorption by 6-line ferrihydrite, particularly in the system containing 0.84 mmol/L Ca^{2+} and 23.6 μmol/L SO_4^{2-}, a similar adsorption pattern can be observed. Both systems exhibited suppressed phosphate adsorption under acidic conditions and enhanced adsorption under alkaline conditions. Although the titration data of the Shimen sample were fitted less satisfactorily than those of the laboratory-synthesized 6-line ferrihydrite, convergence of the model optimization was still achieved (Fig. 8).

Although the titration data of the Shimen sample were fitted less satisfactorily than those of the laboratory-synthesized 6-line ferrihydrite, the model optimization still achieved convergence. Based on the optimized surface-site concentrations, the corresponding site densities were estimated to be $2.00\cdot10^{-2}$ mol site/mol Fe and $2.67\cdot10^{-3}$ mol site/mol Fe for the laboratory-synthesized 6-line ferrihydrite and the Shimen sample, respectively. Despite the substantially lower density of reactive surface sites in the Shimen sample, its maximum phosphate adsorption capacity was comparable to that of the synthesized ferrihydrite. This observation suggests that phosphate retention may involve mechanisms beyond the three classical surface complexation species considered in the model. The optimized protonation (pK_{a1}) and deprotonation constants (pK_{a2}) for the Shimen sample were 3.55 and − 9.05, respectively. Comparison with the titration data of hydrous ferric oxide (HFO) reported by Davis (1977) and Hsi and Langmuir (1985), which were fitted using the same modeling approach, indicates a point of zero charge (PZC) of approximately 7.9 for HFO. In contrast, the Shimen sample exhibited a PZC near pH 6.2 (Fig. 8). Its titration behavior was more comparable to that of the Si-bearing ferrihydrite synthesized by Rancourt et al. (1993), who reported a PZC of 5.8 (Fig. 8). Therefore, the synergistic effects of coexisting ions and differences in surface-reactive sites are likely the primary factors responsible for the distinct phosphate adsorption envelopes observed between the Shimen sample and the laboratory-synthesized 6-line ferrihydrite.

4 Conclusions

Based on laboratory-synthesized ferrihydrite, surface protonation/deprotonation properties and phosphate adsorption behaviors were investigated and compared with those of a natural ferrihydrite sample. The main conclusions are summarized as follows.

The surface protonation and deprotonation constants of the synthesized ferrihydrite were $pKa_1 = 6.80$ and $pKa_2 = -9.93$, respectively, with a point of zero charge (PZC) of 8.5 and a reactive surface-site density of $2.00\cdot10^{-2}$ mol site/mol Fe. Sulfate and arsenate inhibited phosphate adsorption across the entire adsorption envelope, resulting in average reductions of approximately 10–20% and 18–48%, respectively, indicating that arsenate exerted a substantially stronger competitive effect than sulfate. In contrast, Ca^{2+} enhanced phosphate adsorption, particularly under alkaline conditions, where adsorption

increased by up to 65% in the presence of 0.84 mmol/L Ca^{2+}. Furthermore, the combined presence of Ca^{2+} and SO_4^{2-} produced a synergistic enhancement of phosphate retention, with phosphate adsorption increasing by approximately 70–90% at elevated Ca^{2+} and SO_4^{2-} concentrations.

The phosphate adsorption envelope of the natural ferrihydrite sample differed markedly from that of the laboratory-synthesized material. The corresponding surface protonation and deprotonation constants were pKa_1 = 3.55 and pKa_2 = −9.05, respectively, and the PZC was approximately 6.2. The coexistence of calcium and sulfate was identified as the primary factor responsible for the variation in adsorption behavior. Therefore, the influence of coexisting ions should be carefully considered when evaluating phosphate adsorption and retention by natural ferrihydrite-rich materials.

Declarations

Ethical Approval

This is not applicable.

Consent to Participate

This is not applicable.

Consent to Publish

This is not applicable.

Competing Interests

The authors declare that they have no competing interests.

Funding

This work was supported by the Sichuan Province Science and Technology Support Program (2024ZYD0042).

Author Contribution

Authors' Contributions Jing LIU: Writing – original draft, review & editing, Data curation, Visualization, Validation, Methodology, Investigation, Funding acquisition, Conceptualization.Shu Chen: Writing – review & editing, Visualization, Funding acquisition, Project administration, Resource.

Acknowledgements

We gratefully acknowledge Prof. Yun-Gui Li of Southwest University of Science and Technology for providing the FITEQL user manual and Prof. Weiqing Wang for valuable discussions and insights regarding the modeling.

Data Availability Statement

The data supporting the findings of this study are available from the corresponding author upon reasonable request.

References

1. Antelo J, Arce F, Fiol S (2015) Arsenate and phosphate adsorption on ferrihydrite nanoparticles: Synergetic interaction with calcium ions. Chem Geol 410:53–62. https://doi.org/10.1016/j.chemgeo.2015.06.011
2. Clesceri LS, Greenberg AE, Trussell RR (1989) Standard Methods for the Examination of Water and Wastewater, 17th edn. American Public Health Association, Washington, DC
3. Cornell RM, Schwertmann U (2003) Synthesis. In: Cornell RM, Schwertmann U (eds) The Iron Oxides: Structure, Properties, Reactions, Occurrences and Uses, 2nd edn. Wiley-VCH, Weinheim, pp 527–542
4. Davis JA (1977) The structure of the oxide/aqueous electrolyte interface. Ph.D. dissertation, Stanford University, Stanford, CA, USA
5. Davis JA (1978) Surface ionization and complexation at the oxide/water interface. II. Surface properties of amorphous iron oxyhydroxide and adsorption of metal ions. J Colloid Interface Sci 67:90–107. https://doi.org/10.1016/0021-9797(78)90217-5
6. Davies SHR (1987) Mn(II) oxidation in the presence of lepidocrocite: The influence of other ions. In: Davis, J.A., Hayes, K.F. (Eds.), Geochemical Processes at Mineral Surfaces. ACS Symposium Series, Vol. 323, pp 487–502
7. Dzombak DA, Morel FMM (1990) Surface Complexation Modeling: Hydrous Ferric Oxide. Wiley, New York
8. Fan L, Zhao F, Liu J et al (2018) The As behavior of natural arsenical-containing colloidal ferric oxyhydroxide reacted with sulfate reducing bacteria. J Environ Chem Eng 332:183–191. https://doi.org/10.1016/j.cej.2017.09.078
9. Gao Y, Mucci A (2001) Acid-base reactions, phosphate and arsenate complexation, and their competitive adsorption at the surface of goethite in 0.7 M NaCl solution. Geochim Cosmochim Acta 65:2361–2378. https://doi.org/10.1016/S0016-7037(01)00589-0
10. Gauthier J (2011) Modeling the Adsorption of Phosphate in Agricultural Soils of Southern Ontario. MSc Thesis. University of Guelph, Guelph, Canada

11. Goldberg S (1985a) Chemical modeling of anion competition on goethite using the constant capacitance model. Soil Sci Soc Am J 49:851–856. https://doi.org/10.2136/sssaj1985.03615995004900040013x
12. Goldberg S (1985b) Chemical modeling of arsenate adsorption on aluminum and iron oxide minerals. Soil Sci Soc Am J 50:1154–1157. https://doi.org/10.2136/sssaj1986.03615995005000050012x
13. Goldberg S, Sposito G (1984a) A chemical model of phosphate adsorption by soils. I. Reference oxide minerals. Soil Sci Soc Am J 48:772–778. https://doi.org/10.2136/sssaj1984.03615995004800040015x
14. Goldberg S, Sposito G (1984b) A chemical model of phosphate adsorption by soils. II. Noncalcareous soils. Soil Sci Soc Am J 48:779–783. https://doi.org/10.2136/sssaj1984.03615995004800040016x
15. Hawke D, Carpenter PD, Hunter KA (1989) Competitive adsorption of phosphate on goethite in marine electrolytes. Environ Sci Technol 23:187–191
16. https://doi.org/10.1021/es00179a008
17. Hayes KF, Papelis C, Leckie JO (1988) Modeling ionic strength effects on ionic adsorption at hydrous oxide/solution interfaces. J Colloid Interface Sci 125:717–726. https://doi.org/10.1016/0021-9797(87)90078-6
18. Herbelin AL, Westall JC (1999) FITEQL 4.0: A computer program for determination of chemical equilibrium constants from experimental data. Report 99 – 01, Department of Chemistry, Oregon State University, Corvallis, OR, USA
19. Hiemstra T (2013) Surface and mineral structure of ferrihydrite. Geochim Cosmochim Acta 105:316–325. https://doi.org/10.1016/j.gca.2012.12.002
20. Hiemstra T, Zhao W (2016) Reactivity of ferrihydrite and ferritin in relation to surface structure, size, and nanoparticle formation studied for phosphate and arsenate. Environ Sci Nano 3:1265–1279. https://doi.org/10.1039/c6en00061d
21. Hiemstra T, van Riemsdijk WH (1996) A surface structural approach to ion adsorption: The charge distribution model. J Colloid Interface Sci 179:488–508. https://doi.org/10.1006/jcis.1996.0242
22. Hiemstra T, van Riemsdijk WH (2009) A surface structural model for ferrihydrite I: Sites related to primary charge, molar mass, and mass density. Geochim Cosmochim Acta 73:4423–4436. https://doi.org/10.1016/j.gca.2009.04.032
23. Hsi CD, Langmuir D (1985) Adsorption of uranyl onto ferric oxyhydroxides: Application of the surface complexation site-binding model. Geochim Cosmochim Acta 49:1931–1941. https://doi.org/10.1016/0016-7037(85)90088-2
24. Loannou Z, Dimirkou A, Ioannou A (2013) Adsorption from aqueous solutions onto goethite, bentonite and bentonite-goethite systems. Water Air Soil Pollut 224:1374. https://doi.org/10.1007/s11270-012-1374-3

25. Kanematsu M, Young TM, Fukushi K et al (2010) Extended triple-layer modeling of arsenate and phosphate adsorption on a goethite-based granular porous adsorbent. Environ Sci Technol 44:3388–3394. https://doi.org/10.1021/es903658h
26. Kanematsu M, Young TM, Fukushi K et al (2011) Quantification of the effects of organic and carbonate buffers on arsenate and phosphate adsorption on a goethite-based granular porous adsorbent. Environ Sci Technol 45:561–568. https://doi.org/10.1021/es1026745
27. Liang Y, Jin JJ, Chen HF et al (2024) Modeling of phosphate speciation on goethite surface: Effects of humic acid. Chemosphere 359:142351. https://doi.org/10.1016/j.chemosphere.2024.142351
28. Liu S, Jing C, Meng X (2008) Arsenic re-mobilization in water treatment adsorbents under reducing conditions: Part II. XAS and modeling study. Sci Total Environ 392:137–144. https://doi.org/10.1016/j.scitotenv.2007.10.033
29. Mendez JC, Hiemstra T (2019) Carbonate adsorption to ferrihydrite: Competitive interaction with phosphate for use in soil systems. ACS Earth Space Chem 3:129–141. https://doi.org/10.1021/acsearthspacechem.8b00160
30. Mendez JC, Hiemstra T, Koopmans GF (2020) Assessing the reactive surface area of soils and the association of soil organic carbon with natural oxide nanoparticles using ferrihydrite as proxy. Environ Sci Technol 54: 11990–12000. https://doi.org/0.1021/acs.est.0c02163
31. Mesuere K, Fish W (1992) Chromate and oxalate adsorption on goethite. I. Calibration of surface complexation models. Environ Sci Technol 26:2357–2364. https://doi.org/10.1021/es00036a004
32. Michel FM, Barrón V, Torrent J et al (2010) Ordered ferrimagnetic form of ferrihydrite reveals links among structure, composition, and magnetism. Proc Natl Acad Sci U S A 107:2787–2792. https://doi.org/10.1073/pnas.091017010
33. Nilsson N, Persson P, Lövgren L (1996) Competitive surface complexation of o-phthalate and phosphate on goethite (α-FeOOH) particles. Geochim Cosmochim Acta 60:4385–4395. https://doi.org/10.1016/S0016-7037(96)00258-X
34. Nowack B, Stone AT (2006) Competitive adsorption of phosphate and phosphonates onto goethite. Water Res 40:2201–2209. https://doi.org/10.1016/j.watres.2006.03.018
35. Rancourt L (1993) Adsorption of Arsenate Ions on Iron Oxohydroxides. MSc Thesis. Université du Québec, Québec, Canada
36. Ren X, Yan N, Chen S et al (2022) Remediation of arsenic-containing ferrihydrite in soil using iron- and sulfate-reducing bacteria: Implications for microbially-assisted clean technology. J Environ Chem Eng 10(6):108876. https://doi.org/10.1016/j.jece.2022.108876
37. Talebi M, Rahnemaie R, Goli Kalanpa E et al (2016) Competitive adsorption of magnesium and calcium with phosphate at the goethite-water interface: Kinetics, equilibrium and CD-MUSIC modeling. Chem Geol 437:19–29. https://doi.org/10.1016/j.chemgeo.2016.05.004
38. Tejedor-Tejedor MI, Anderson MA (1990) Protonation of phosphate on the surface of goethite as studied by CIR-FTIR and electrophoretic mobility. Langmuir 6:602–611. https://doi.org/10.1021/la00093a015

39. Tiberg C, Sjöstedt C, Eriksson AK (2020) Phosphate competition with arsenate on poorly crystalline iron and aluminum (hydr)oxide mixtures. Chemosphere 255:126937. https://doi.org/10.1016/j.chemosphere.2020.126937
40. Venema P, Hiemstra T, van Riemsdijk WH (1997) Interaction of cadmium with phosphate on goethite. J Colloid Interface Sci 192:94–103. https://doi.org/10.1006/jcis.1997.4988
41. Verbeeck M, Hiemstra T, Thiry Y (2017) Soil organic matter reduces the sorption of arsenate and phosphate: A soil profile study and geochemical modelling. 68:678–688. https://doi.org/10.1111/ejss.12447
42. Wang X, Li W, Harrington R et al (2013) Effect of ferrihydrite crystallite size on phosphate adsorption reactivity. Environ Sci Technol 47:10322–10331. https://doi.org/10.1021/es401301z
43. Weng L, van Riemsdijk WH, Hiemstra T (2012) Factors controlling phosphate interaction with iron oxides. J Environ Qual 41:628–635. https://doi.org/10.2134/jeq2011.0250
44. Xu W, Hausner DB, Harrington R et al (2011) Structural water in ferrihydrite and constraints this provides on possible structure models. Am Mineral 96:513–520. https://doi.org/10.2138/am.2011.3460

Figures

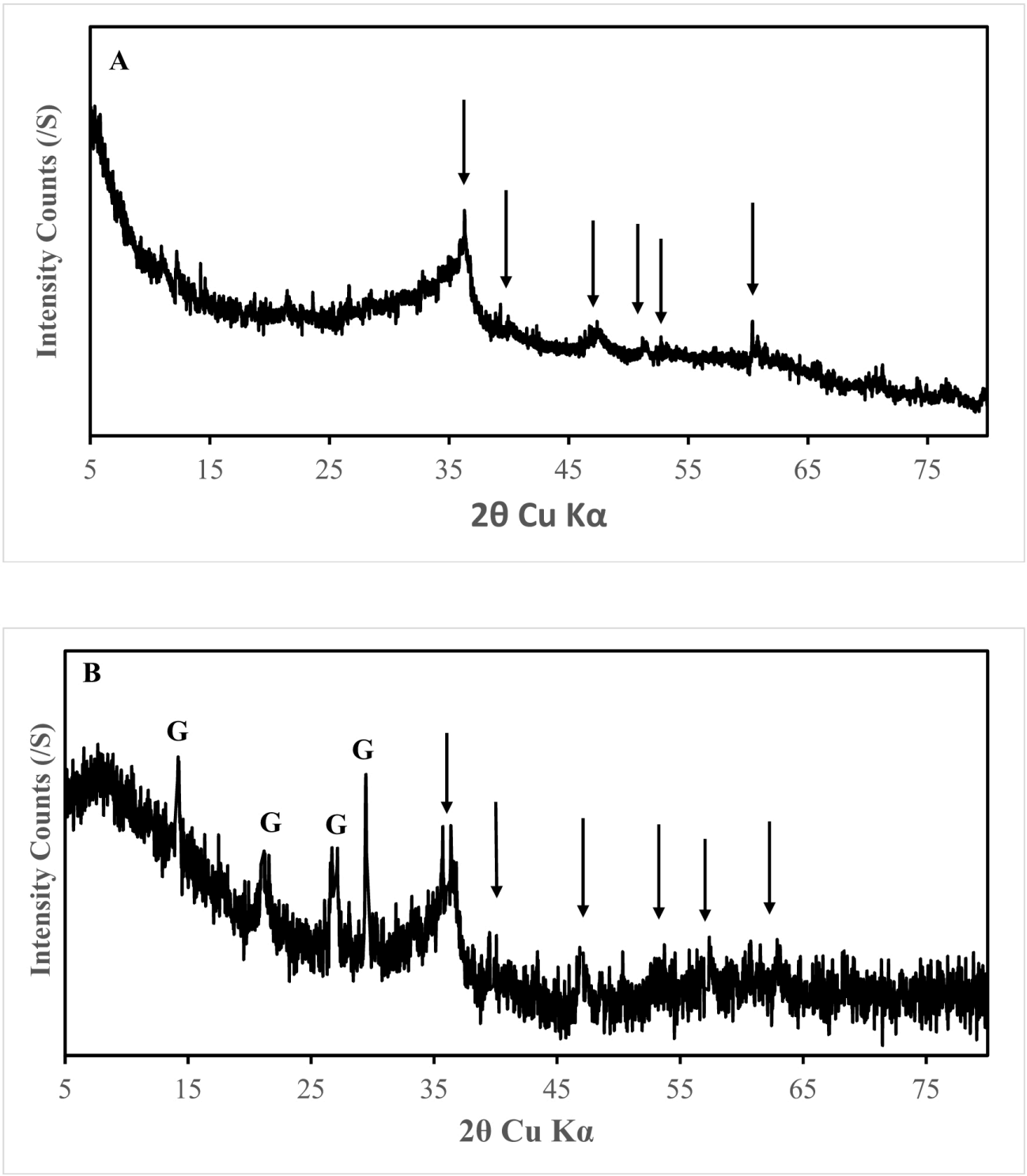

Figure 1

The X-ray diffraction diagram of synthetic 6-line ferrihydrite and collected samples from Shimen Realgar mine, Changde City, China.

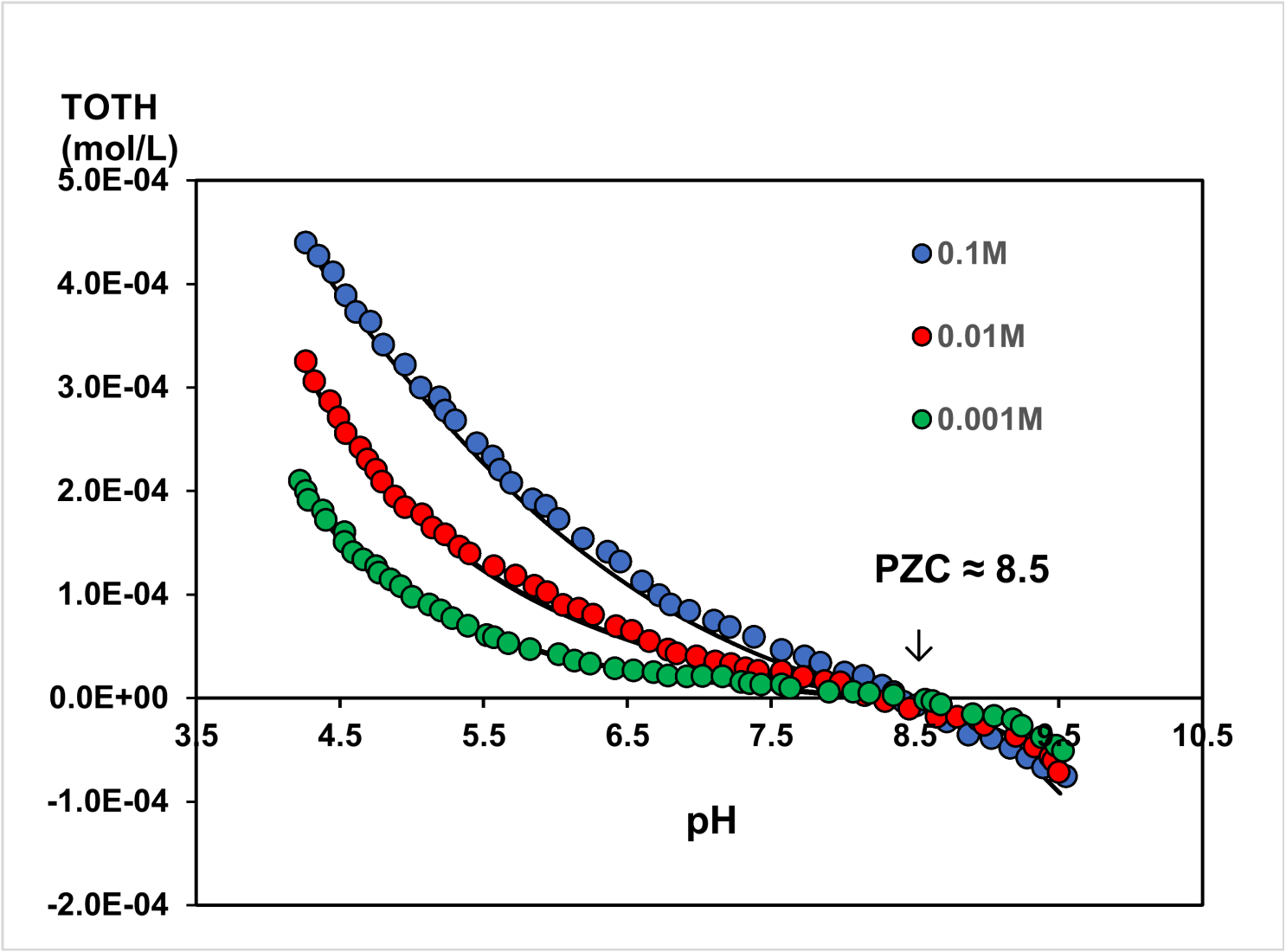

Figure 2

Titratation curve of 6-lines ferrihydrite. Circles are experimental data and lines are calculated by FITEQL (2.4 g/L, C_1=1.05 F/m^2, surface area=115 m^2/g)

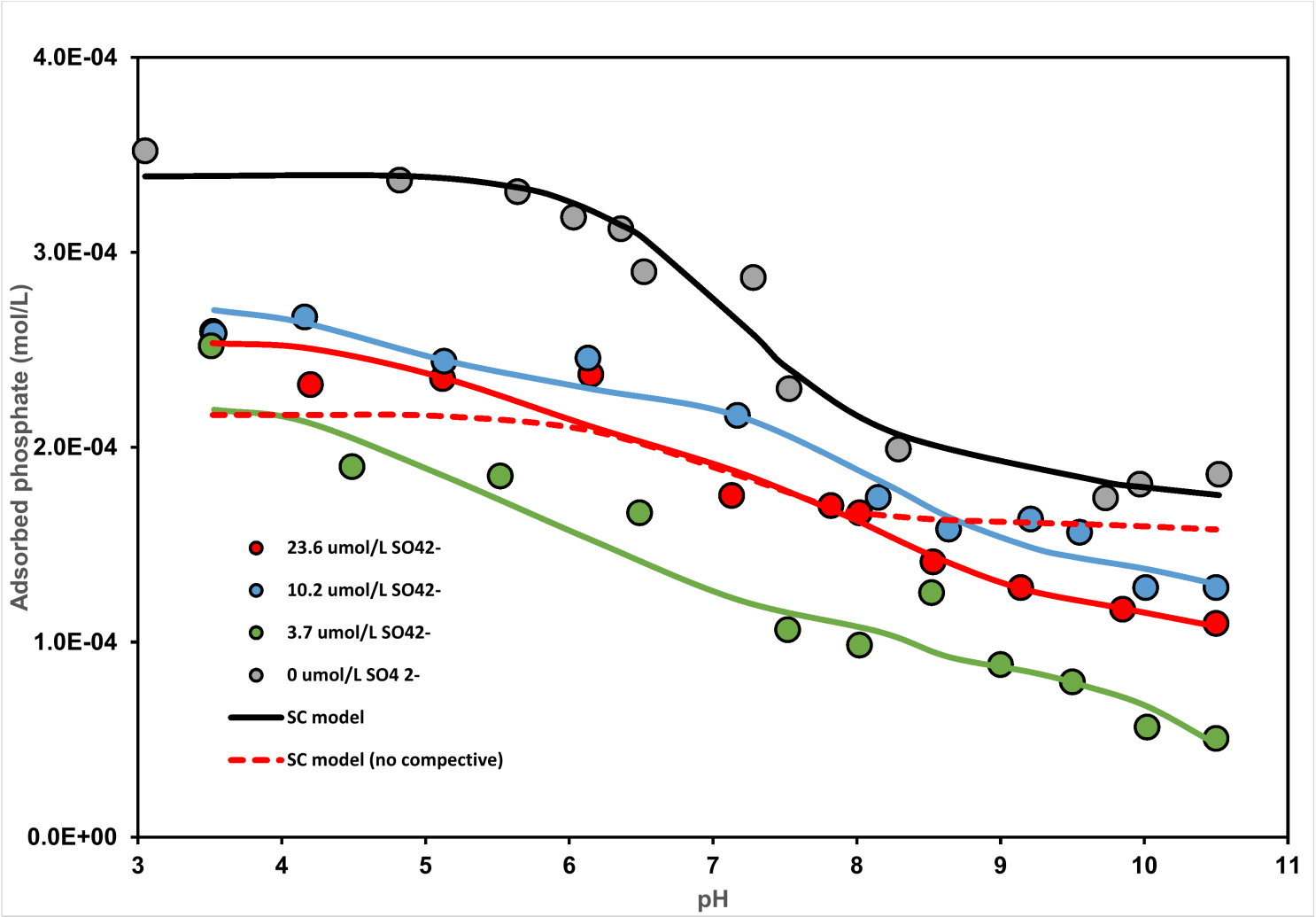

Figure 3

Adsorption envelope of phosphate on 6-lines ferrihydrite under various concentration of sulfate. Various color lines refer to the predicted adsorption equilibrium concentrations in competition experiments using the SCM model with the parameters given in the tables 1. Red dotted line refers to the SCM model without competitive mechanisms for comparison.

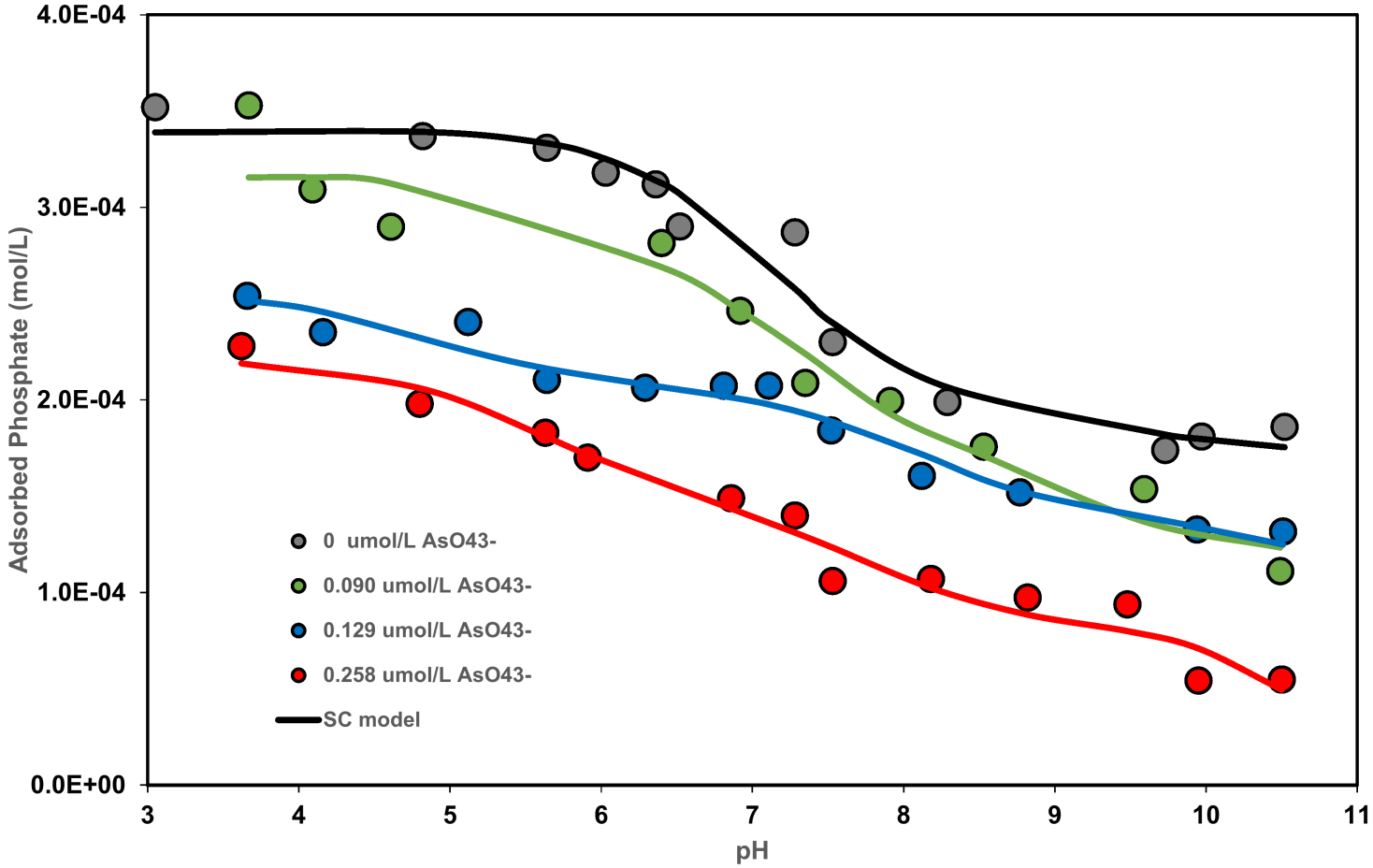

Figure 4

Adsorption envelope of phosphate on 6-lines ferrihydrite under various concentration of arsenate. Various color lines refer to the predicted adsorption equilibrium concentrations in competition experiments using the SCM model with the parameters given in the tables 1.

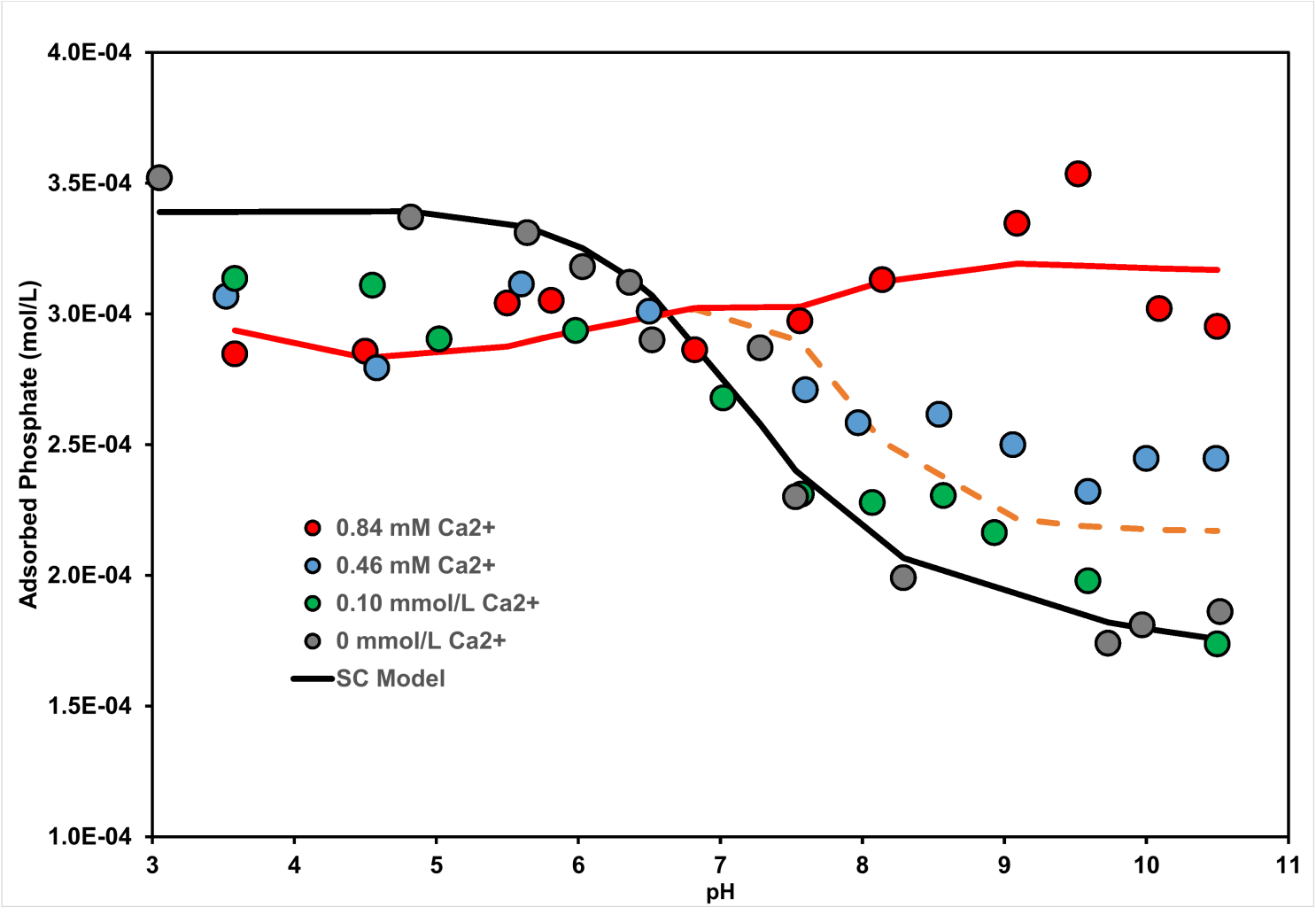

Figure 5

Adsorption envelope of phosphate on 6-lines ferrihydrite under various concentration of calcium. Various color lines refer to the predicted adsorption equilibrium concentrations in competition experiments using the SCM model with the parameters given in the tables 1.

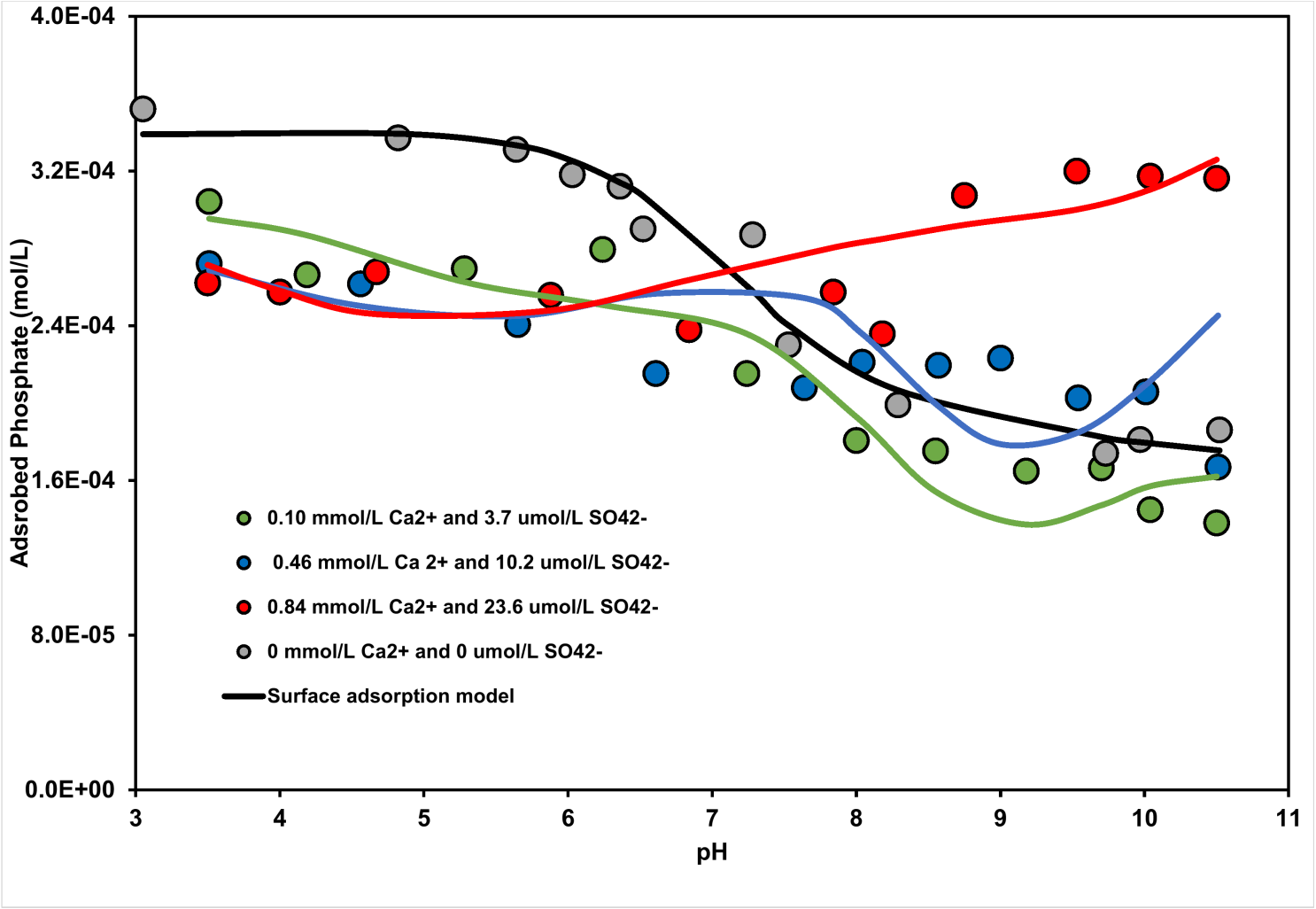

Figure 6

Adsorption envelope of phosphate on 6-lines ferrihydrite under various concentration of calcium and sulfate. Various color lines refer to the predicted adsorption equilibrium concentrations in competition experiments using the SCM model with the parameters given in the tables 1.



Figure 7

Occurrence of 6-line ferrihydrite and gypsum in samples from the Shimen mining area. Brown aggregates correspond to ferrihydrite, while the transparent needle-like crystals are gypsum. Photograph by Jing.

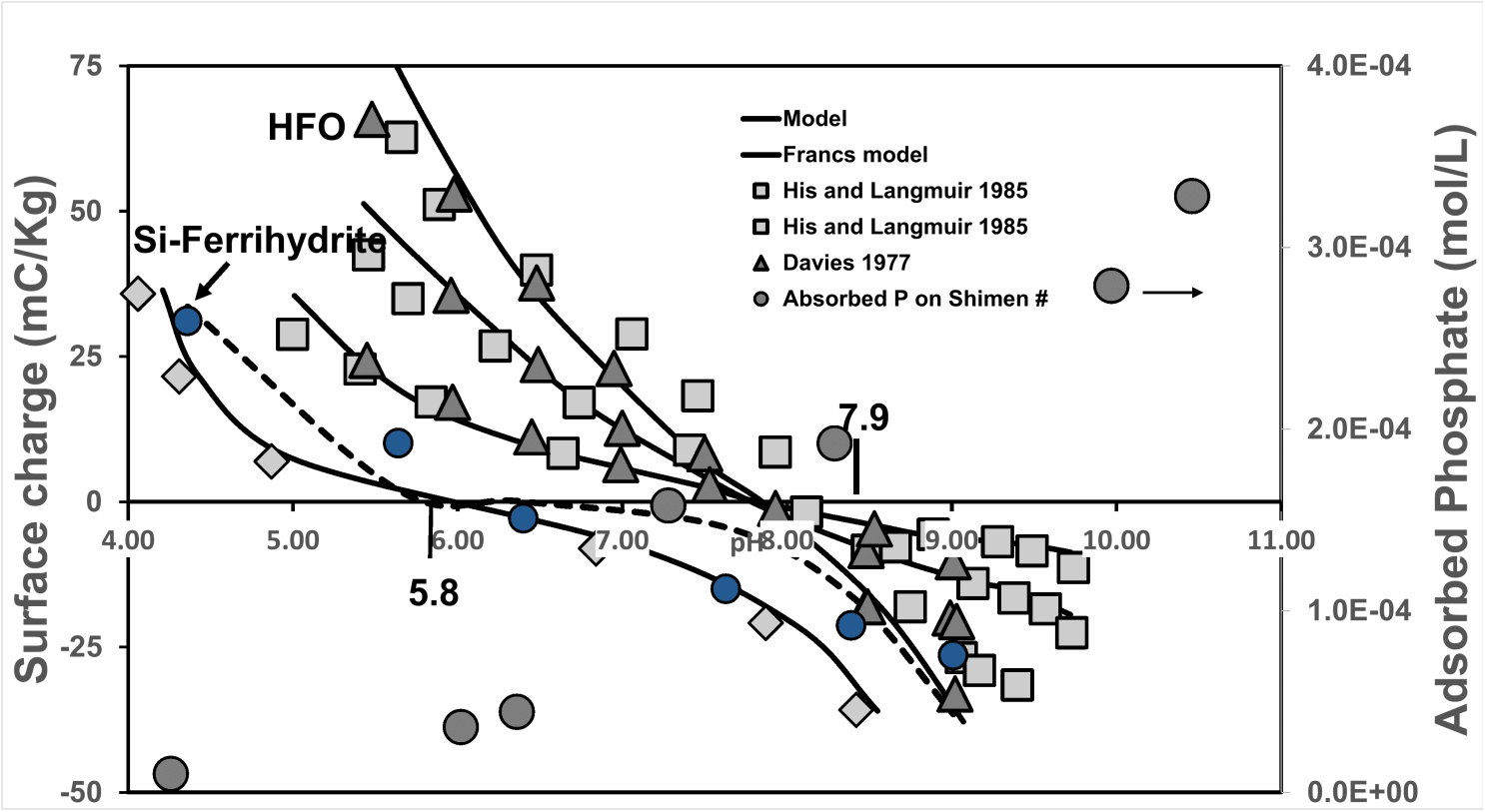

Figure 8

Surface charge per unit mass (mC/Kg) of HFO, Si-Ferrihydrite and 6-lines ferrihydrite from Shimen mine area as a function of pH in 0.01 M $NaNO_3$ (Left axis) and Phosphate envelope on Shimen sample (Right axis). Symbols show experimental data of ref. (His and Langmuir, 1985; Lise Rancourt 1993) and titration data of filed ferrihydrite in this study. The lines show prediction with the CCM model of FITEQL based on above these experimental data.